SAND 2007-3373J

Revised Thermodynamic Properties of Brucite Determined by Solubility Studies and Its Significance to Nuclear Waste Isolation

Yongliang Xiong[1]

Sandia National Laboratories (SNL)*
Carlsbad Programs Group
4100 National Parks Highway, Carlsbad, NM 88220, USA

[1] Corresponding author, e-mail: yxiong@sandia.gov.

* Sandia National Laboratories is a multiprogram laboratory operated by Sandia Corporation, a Lockheed Martin Company, for the United States Department of Energy's National Nuclear Security Administration under Contract DE-AC04-94AL85000.

ABSTRACT

Solubility experiments were conducted for the dissolution reaction of brucite, $Mg(OH)_2$ (cr):

$$Mg(OH)_2\ (cr) + 2H^+ = Mg^{2+} + 2H_2O$$

Experiments were conducted from undersaturation in deionized (DI) water and 0.01 M–4.0 M NaCl solutions at room temperature. In addition, brucite solubility was measured from supersaturation in a single experiment in which brucite was precipitated via drop-wise addition of 0.1 m NaOH into a 0.1 m $MgCl_2$ solution. The solubility constant at infinite dilution calculated from the experimental results in DI water and 0.01 M NaCl solution using the Davies equation is:

$$\log K_s^o = 17.2\pm0.3\ (2\sigma)$$

The $\log K_s^o$ obtained from the supersaturation results by using the specific interaction theory (SIT) is 17.1±0.4 (2σ).

By using known Pitzer interaction parameters, the experimental results in the 0.01 M to 4.0 M NaCl solutions were modeled with the computer code NONLIN. According to the modeling, the dimensionless standard chemical potential (μ^o/RT) of brucite is –335.36±0.69 (2σ), with the corresponding Gibbs free energy of formation of brucite, $\Delta_f G^o_{298,brucite}$, being –831.3±1.9 (2σ) kJ mol^{-1}. In combination with the auxiliary thermodynamic data of CODATA, the $\log K_s^o$ is calculated to be 17.2±0.3 (2σ) based on the above derived Gibbs free energy of formation for brucite. The above three activity coefficient models give a consistent solubility constant when modeling the results of the different experiments.

INTRODUCTION

An accurate knowledge of the thermodynamic properties of brucite ($Mg(OH)_2$) is critical for understanding its importance in nuclear waste isolation. Brucite has become significant to waste isolation projects due to its use in engineered barriers for nuclear waste repositories. Crystalline MgO, which hydrates rapidly to brucite, is the only engineered barrier certified by the US Environmental Protection Agency (EPA) at the Waste Isolation Pilot Plant (WIPP) located near Carlsbad, New Mexico, USA (e.g., Krumhansl et al., 2000; Xiong and Snider, 2003; Xiong and Lord, 2006). An $Mg(OH)_2$-based engineered barrier is also proposed for the German Asse salt mine repository (Schüessler et al., 2002). The geochemical functions of the engineered barrier in the WIPP are (1) to consume CO_2 possibly produced by microbial degradation of organic materials in waste packages, and (2) to buffer the pH and f_{CO_2} of the repository (Krumhansl et al., 2002; Xiong and Snider, 2003). Experimental work at Sandia National Laboratories conducted at room temperature and atmospheric P_{CO_2} indicates that MgO first hydrates to brucite, which in turn is carbonated to form hydromagnesite (5424) ($Mg_5(CO_3)_4(OH)_2 \bullet 4H_2O$) (Xiong and Snider, 2003). Consequently, the thermodynamic properties of the brucite-hydromagnesite (5424) assemblage are of great significance to the performance assessment (PA) because actinide solubility is strongly affected by f_{CO2}. In addition, PA is important to the demonstration of the long-term safety of nuclear waste repositories, as assessed by the use of probabilistic performance calculations.

A literature review of the thermodynamic properties of brucite shows that there is a substantial discrepency in the values of $\Delta_f G^\circ_{brucite}$ reported in the literature. These values range from –830.4 (Harvie et al., 1984), –831.9 (Brown et al., 1996), –833.5

(Robie and Hemingway, 1995), to –835.9 kJ mol^{-1} (Konigsberger et al., 1999). Using the $\Delta_f G^\circ_{hydromagnesite\ (5424)}$ from Konigsberger et al. (1999), the predicted $\log f_{CO2}$ in equilibrium with the assemblage brucite–hydromagnesite (5424) would range from –5.96 ($\Delta_f G^\circ_{brucite}$ from Harvie et al., 1984) to –4.84 ($\Delta_f G^\circ_{brucite}$ from Konigsberger et al., 1999). The above discussion shows that a much better constrained value for $\Delta_f G^\circ_{brucite}$ is required to accurately assess the role of brucite in nuclear waste repositories. For this reason, a series of solubility experiments involving brucite in NaCl solutions ranging from 0.01 M to 4.0 M were conducted at room temperature. These experiments were used to derive new values of $\Delta_f G^\circ_{brucite}$ by extrapolation to infinite dilution via Pitzer formalism. A similar study conducted by the Institut für Nukleare Entsorgung (Altmaier et al., 2003) show results consistent with those reported in this study, initially summarized and reported in 2003 (Xiong, 2003). The results obtained in this study are also used to demonstrate the significance of the thermodynamic properties of brucite in nuclear waste isolation by performing calculations of important geochemical parameters such as pH.

METHODOLOGY

All materials (NaCl, $MgCl_2 \cdot 6H_2O$, $Mg(OH)_2$, NaOH) used in this study are reagent grade from Fisher Scientific. Deionized (DI) water with 18.3 MΩ was produced by a *NANOpure Infinity Ultra Pure Water System* from Barnstead. Degassed DI water was used for preparation of all starting solutions. The degassed DI water was obtained by bubbling high purity argon gas (purity 99.996%) from AIR GAS, inc. through DI water for at least one hour, following a procedure similar to that described by Wood et al. (2002). Starting solutions were prepared such that the equilibrium solubility was

approached from both under- and supersaturation with respect to brucite. For the undersaturated experiments the starting solutions included DI water and NaCl solutions ranging from 0.01 to 4.0 M NaCl. The supersaturation experiment used a 0.1 m $MgCl_2$ starting solution.

All experiments were conducted at room temperature (22.5 ± 1.5 °C). For each of the experiments undersaturated with respect to brucite, 5 grams of $Mg(OH)_2$ (cr) was placed into a 30-mL Oak Ridge centrifuge tube containing 30 grams of starting solution (NaCl solution or DI water). In order to determine the equilibrium brucite solubility from the direction of supersaturation, about 450 mL of 0.1 m $MgCl_2$ solution was placed in a 500 mL polyethylene bottle. Brucite was subsequently precipitated from the solution via drop-wise addition of a 0.1 m NaOH solution. All experiments (both under- and supersaturation) were placed on an INNOVA 2100 Platform Shaker (New Brunswick Scientific, Inc.) at a shaking speed of 140 RPM for the duration of the experiments.

At specific intervals, the pH of each experimental solution was measured with an Orion-Ross combination pH glass electrode. Before each measurement, the pH meter was calibrated with three pH buffers (pH 4, pH 7 and pH 10). For solutions with ionic strengths higher than 0.1 M, the observed solution pH values were converted to hydrogen-ion concentrations (pcH) using a correction factor, A (see below).

The relation between the pH electrode reading (pH_{ob}) and pcH can be expressed as (Rai et al., 1995):

$$pcH = pH_{ob} + A \qquad (1)$$

The correction factor, A, is defined as:

$$A = \log \gamma_{H^+} + (F/2.303RT)\, \Delta E_j \qquad (2)$$

where γ_{H^+} is the conventional activity coefficient of H^+, F is Faraday constant, R is the gas constant, T is the temperature in Kelvin, and ΔE_j is the difference in liquid junction potential between standards and solution. Both terms on the right-hand side of Eq. (2) are not independently measurable, but the combination can be determined.

Rai et al. (1995) conducted extensive studies to investigate the correction factors (A) in concentrated NaCl and Na_2SO_4 electrolytes for various Orion-Ross combination electrodes. The linear relation between A values and concentrations for NaCl solutions obtained by Rai et al. (1995), is expressed as:

$$A = 0.159X \tag{3}$$

where X is the NaCl concentration in molality. This expression is valid for NaCl solutions up to 6.0 m in concentration. They also performed a study to evaluate the dependence of the A values on an individual electrode by using a number of different Orion-Ross electrodes. They concluded that there is no significant difference in A values for different electrodes and that the linear relation between A values and concentrations of NaCl and Na_2SO_4 obtained can be applied to different NaCl and Na_2SO_4 solutions. Therefore each electrode does not need to be individually calibrated.

After a pH measurement was taken, approximately 3 mL of solution was withdrawn from an experimental run. The solution was filtered using a 0.2 μm syringe filter. The filtered solution was then weighed and acidified with 0.5 mL of concentrated HNO_3 (TraceMetal grade from Fisher Scientific). The extracted solution was then diluted to 10 mL with DI water so that dissolved ΣMg^{2+} and Na^+ concentrations could be determined. Using a technique successfully demonstrated by Xiong and Wood (1999; 2001), the steady state conditions were intentionally disturbed by recharging each

experimental run from the direction of undersaturation. The purpose of recharging is to monitor whether the equilibrium is attained (Xiong and Wood, 1999; 2001). This was accomplished by adding fresh matrix solution in approximately the same amount that was withdrawn after completing three or four samplings. In subsequent sampling(s), deviations in the solution chemistry from the previous samplings were not observed. This suggests that the experiments successfully re-equilibrated after each recharge. Because the experimental runs were periodically recharged with matrix solutions, the results should not be used for kinetic studies.

The chemical analyses of solutions were performed with a Perkin Elmer dual-view inductively coupled plasma-atomic emission spectrometer (ICP-AES) (Perkin Elmer DV 3300). Calibration blanks and standards were precisely matched with experimental matrices. The correlation coefficients of calibration curves in all measurements were better than 0.9995. The analytical precision is better than 1.00% in terms of the relative standard deviation (RSD) based on replicate analyses.

Solid phase identification was performed by using the Brucker X-ray Diffraction. There is no new phase observed.

EXPERIMENTAL RESULTS

Results for the experimental runs starting with DI water and 0.01 M NaCl solution are listed in Table 1. Experimental results from the supersaturated run (0.1 m $MgCl_2$ starting solution) are tabulated in Table 2. All other experimental results are tabulated in Table 3. In Figure 1, a plot of log $m_{\Sigma Mg}/(m_{H^+})^2$ versus time is shown for the 0.1 M NaCl experiment that approached equilibrium from undersaturation with respect to brucite.

The plot in Figure 1 also shows the results for the supersaturation experiment in which brucite was precipitated from a 0.1 m $MgCl_2$ solution. Because these two experimental runs have similar ionic strengths (I = 0.105 m to 0.114 m for the 0.1 M NaCl experiment; and I = 0.242 m to 0.269 m for the 0.1 m $MgCl_2$ experiment), the consistent results from these sets of experiments indicate that the reversal was attained (Figure 1). All other results are plotted in Figure 2. The molar concentration of the 0.1 M NaCl solution was converted to a molal scale by using the conversion factor recommended by Grenthe et al. (1992). The ionic strength of the experiment with the 0.1 m $MgCl_2$ solution from which brucite was precipitated by drop-wise addition of 0.1 m NaOH was calculated using the Na and Mg concentrations determined by ICP-AES, and the original Cl concentration:

$$I_m = \frac{1}{2}(2^2 \times m_{Mg} + 1^2 \times m_{Na} + 1^2 \times m_{Cl}) \quad (4)$$

In order to obtain thermodynamic properties for brucite from the experimental results discussed above, the solubility data needs to be extrapolated to infinite dilution. For the very low ionic strength experiments (those starting with DI water and 0.01 M NaCl) the Davies equation (Davies, 1938) was used to extrapolate the experimentally determined equilibrium quotients (Table 1) to infinite dilution. The results from the supersaturated experiment (Table 2) were extrapolated to infinite dilution using the Specific Interaction Theory (SIT) interaction coefficients estimated by Xiong (2006). Data from the higher ionic strength experimental runs in 0.1 to 4.0 M NaCl solutions (Table 3) were extrapolated to infinite dilution by using the Pitzer equations as employed in the computer code NONLIN (Felmy, 1990; Babb et al., 1996).

The results obtained from the extrapolations using the Davies equation and the SIT model to infinite dilution are the equilibrium constants for the brucite dissolution reaction:

$$Mg(OH)_2\ (s) + 2H^+ = Mg^{2+} + 2H_2O \qquad (5)$$

The extrapolations made with the Pitzer equations via the NONLIN code give the dimensionless standard chemical potential (μ^o/RT) of brucite, which can be converted to the standard Gibbs free energy of formation of brucite ($\Delta_f G$). These values can then be used in conjunction with the μ^o/RT or $\Delta_f G$ values for each of the aqueous species in Eq. (5) to calculate the dissolution constant of brucite.

In the Davies equation (Davies, 1938), the activity coefficient is calculated from:

$$\log \gamma_i = -A_\gamma z_i^2 \left(\frac{\sqrt{I_m}}{1+\sqrt{I_m}} + 0.3 I_m\right) \qquad (6)$$

where γ_i is the activity coefficient of species *i*; A_γ the Debye-Hückel slope for the activity coefficient (from Helgeson and Kirkham, 1974); z_i the charge of species *i*, and I_m the ionic strength on a molal scale.

According to Xiong (2006), the extrapolation to infinite dilution for the reaction Eq. (4) by using the SIT model is given by:

$$\log K_s^o = \log Q - 2D + \varepsilon(Mg^{2+}, Cl^-)\ I_m - 2\varepsilon(H^+, Cl^-)\ I_m + 2 \log a_{H_2O} \qquad (7)$$

where log Q is an equilibrium quotient for the reaction given by Eq. (5) at a given ionic strength; $\varepsilon(Mg^{2+}, Cl^-)$ and $\varepsilon(H^+, Cl^-)$ are the interaction coefficients of the Brønsted-Guggenheim-Scatchard specific interaction theory recommended by Xiong (2006); a_{H_2O} is activity of water; and D is the Debye-Hückel term.

The Debye-Hückel term is given by:

$$D = \frac{A_\gamma \sqrt{I_m}}{1 + \rho\sqrt{I_m}} \tag{8}$$

where ρ is the minimum distance of approach between ions, which is taken as 1.5 (Ciavatta, 1980).

The activity of water is calculated from the expression (e.g., Guilaumont et al., 2003):

$$\log a_{H2O} = \frac{-\phi \sum_k m_k}{\ln(10) \times 55.51} \tag{9}$$

where ϕ is the osmotic coefficient of the solution and the summation is taken over all solute species k with molality m_K in the solution. For a 1:1 electrolyte in which the contributions from all minor species have been ignored, Eq. (9) can be simplified to:

$$\log a_{H2O} = \frac{-2 \times m_{NX} \times \phi}{\ln(10) \times 55.51} \tag{10}$$

For calculations using the experimental results of the 0.1 m $MgCl_2$ solution, the osmotic coefficient is from Rard and Miller (1981).

The Pitzer interaction parameters used in the NONLIN modeling are listed in Table 4. The molal concentrations of H^+, Na^+, Mg^{2+}, Cl^- and OH^- are used as inputs. Among these, m_{H^+} and $m_{Mg^{2+}}$ are measured values, whereas m_{Na^+} and m_{Cl^-} are the initial concentrations of the starting solutions. The molar scale is converted to the molal scale according to the conversion factors for NaCl solutions compiled by Guillaumont et al. (2003). The OH^- concentrations are calculated by using the measured m_{H^+} and the dissociation quotients of water in NaCl solutions at 25 °C (Busey and Mesmer, 1978).

The results in Tables 1-2 and 5 suggest that the solubility constants calculated from three activity coefficient models are in excellent agreement within the given uncertainty.

DISCUSSIONS AND APPLICATIONS

The logarithmic solubility constants obtained in this study are 17.2±0.3 (2σ) for the undersaturation experiments and 17.1±0.4 (2σ) for the supersaturation experiment. These results are in excellent agreement with the logarithmic solubility constant of 17.1±0.2 (2σ) reported by Altmaier et al. (2003).

The change in enthalpy for the brucite dissolution reaction (Eq. 5) is given as -112 kJ mol^{-1} by Brown et al. (1996). Based on this value and the auxiliary enthalpy data from CODATA for Mg^{2+}, H^+, and H_2O (Cox et al., 1989), a $\Delta_f H^o_{298,brucite}$ value of –926.7 kJ mol^{-1} can be derived:

$$\Delta_r H = \Delta_f H^o_{Mg2+} + 2\Delta_f H^o_{H2O} - \Delta_f H^o_{brucite} - 2\Delta_f H^o_{H+} \quad (10)$$

Using the $\Delta_f G^o_{298,brucite}$ derived from this study in combination with the auxiliary thermodynamic data of CODATA for the elements (Cox et al., 1989), the derived $S^o_{298,brucite}$ is 49±6 (2σ) J K^{-1} mol^{-1} according to the Gibbs-Helmholtz equation:

$$\Delta_f G^o = \Delta_f H^o - T\sum_i S^o_j \quad (11)$$

The summation of standard entropies is obtained based on the following reaction:

$$Mg\ (s) + O_2\ (g) + H_2\ (g) = Mg(OH)_2\ (s) \quad (12)$$

In the calculation of the uncertainty propagation for the standard entropy of brucite, only the uncertainties associated with the Gibbs free energy of formation of brucite, and associated with entropies of the elements are considered. As Brown et al. (1996) did not provide the uncertainty for their enthalpy data, the uncertainty propagation for the standard entropy of brucite does not include the uncertainty of enthalpy.

Altmaier et al. (2003) provided detailed descriptions regarding the solubility constants for brucite ($\log K_s^o$) in the literature. In particular, they pointed out that the $\log K_s^o$ (16.30) calculated from the thermodynamic properties selected for brucite in the compilation of Helgeson et al. (1978) is inconsistent with several previous studies and their results. Their assessment is well supported by the present study. It should be emphasized that since the thermodynamic properties for brucite suggested by Helgeson et al. (1978) were included in many databases such as SUP in the EQ3/6 package (Wolery, 1992), revised thermodynamic properties of brucite must be used for modeling systems containing brucite. Otherwise, the predicted pH values may differ from the real values by approximately 0.5 units.

Furthermore, as demonstrated by Xiong and Snider (2003) and Xiong and Lord (2006), the carbonation product of brucite at room temperature is hydromagnesite (5424). Therefore, the $\log f_{CO_2}$ in the repository would be controlled by the equilibrium buffer assemblage of brucite-hydromagnesite (5424), before hydromagnesite (5424) is converted to magnesite. According to the following reaction,

$$5Mg(OH)_2(s) + 4CO_2(g) = Mg_5(CO_3)_4(OH)_2 \cdot 4H_2O(s) \qquad (13)$$

thus if the value of the Gibbs free energy of formation for brucite is changed, the predicted $\log f_{CO_2}$ will be different. In Table 6, the $\log f_{CO_2}$ predicted by using the Gibbs free energy of formation for brucite from this study and from Helgeson et al. (1978) are compared. In these above calculations, the Gibbs free energy of formation for hydromagnesite (5424) is taken from Robie and Hemingway (1995) and the other auxiliary data are taken from Cox et al. (1989). The results in Table 6 show that the

$\log f_{CO_2}$ predicted by using the data for brucite from Helgeson et al. (1978) is higher than that predicted by using the data derived in this study by nearly one order of magnitude.

Since actinides can form strong aqueous complexes with carbonate, this difference may have a significant effect on the solubility of actinides. As an example, the FMT code (Novak, 1996; Babb and Novak, 1997; Wang, 1998; Xiong et al., 2005) was used to calculate the solubility of Am(III) in a 5 M NaCl solution in equilibrium with the brucite-hydromagnesite assemblage (Table 7). As shown in Table 7, if the Gibbs free energy of formation of brucite from Helgeson et al. (1978) was used, the solubility-controlling phase for Am(III) would be $AmCO_3OH(s)$ at the f_{CO_2} ($10^{-4.61}$ bars) buffered by the assemblage brucite-hydromagnesite (5424). In contrast, if the Gibbs free energy of formation of brucite from this study is used, the solubility-controlling phase would be $Am(OH)_3(s)$ at the f_{CO_2} ($10^{-5.50}$ bars) buffered by the assemblage brucite-hydromagnesite (5424). Furthermore, the solubility of Am(III) in the former case is higher than that in the latter case by a factor of 4.6 (Table 7).

SUMMARY

This study recommends that the solubility constant for the brucite dissolution reaction as written in Eq. (4) be 17.2±0.3 (2σ), and the standard Gibbs energy of formation, and standard entropy of brucite be –831.3±1.9 (2σ) kJ mol^{-1} and 49±6 (2σ) J K^{-1} mol^{-1}, respectively.

ACKNOWLEDGEMENTS

Sandia National Laboratories is a multiprogram laboratory operated by Sandia Corporation, a Lockheed Martin Company, for the United States Department of Energy's National Nuclear Security Administration under Contract DE-AC04-94AL85000. This research is funded by WIPP programs administered by the Office of Environmental Management (EM) of the U.S Department of Energy. My thanks are due to Nathalia Chadwick, Kelsey Mae Davis, and Veronica Gonzales, for their laboratory assistance.

REFERENCES

Altmaier, M., Metz, V., Neck, V., Müller, R., Fanghänel, T., 2003. Solid-liquid equilibria of $Mg(OH)_2$(cr) and $Mg_2(OH)_3Cl{\bullet}4H_2O$(cr) in the system Mg–Na–H–OH–Cl–H_2O at 25°C. Geochimica et Cosmochimica Acta 67(19), 3595–3601, doi:10.1016/S0016-7037(03)00165-0.

Babb, S.C., Novak, C.F., 1997. User's manual for FMT version 2.3: A computer code employing the Pitzer Activity Coefficient Formalism for calculating thermodynamic equilibrium in geochemical systems to high electrolyte concentrations [addendum included]. ERMS# 243037. Sandia National Laboratories, WIPP Records Center, Carlsbad, NM.

Babb, S.C., Novak, C.F., Moore, R.C., 1996. WIPP PA (Waste Isolation Pilot Plant Performance Assessment) user's manual for NONLIN, version 2.0. ERMS# 230740. Sandia National Laboratories, WIPP Records Center, Carlsbad, NM.

Brown, P.L., Drummond, S.E., Jr., Palmer, D.A., 1996. Hydrolysis of magnesium (II) at elevated temperatures. Journal of the Chemical Society, Dalton Transactions, July 21, 1996, no. 14, 3071–3075

Busey, R.H., Mesmer, R.E., 1978. Thermodynamic quantities for ionization of water in sodium-chloride media to 300°C. Journal of Chemical and Engineering Data 23(2), 175–176

Ciavatta, L., 1980. The specific interaction theory in evaluating ionic equilibria. Annali di Chimica 70(11-1), 551–567.

Cox, J.D., Wagman, D.D., Medvedev, V.A., 1989. CODATA Key Values for Thermodynamics. Hemisphere Publishing Corporation, NY. Available at http://www.codata.org/resources/databases/key1.html (5/12/07).

Davies, C.W., 1938. The extent of dissociation of salts in water. VIII. An equation for the ionic activity coefficients of an electrolyte in water, and a revision of the dissociation constant of some sulfates. Journal of the Chemical Society, 2093-2098.

Felmy, A.R., 1990. GMIN: A computerized chemical equilibrium model using a constrained minimization of the Gibbs free energy. PNL–7281. Pacific Northwest National Laboratory, Richland, WA.

Grenthe, I., Fuger, J., Konings, R.J.M., Lemire, R.J., Muller, A.B., Nguyen-Trung, C.,Wanner, H., 1992. Chemical Thermodynamics of Uranium. Nuclear Energy Agency, Organisation for Economic Co-Operation and Development, Paris.

Guillaumont, R., Fanghänel, T., Fuger, J., Grenthe, I., Neck, V., Palmer, D.A., Rand, M.H., 2003. Update on the Chemical Thermodynamics of Uranium, Neptunium, Plutonium, Americium and Technetium. Elsevier, Amsterdam.

Harvie, C.E., Møller, N., Weare, J.H., 1984. The prediction of mineral solubilities in natural waters: the Na-K-Mg-Ca-H-Cl-SO_4-OH-HCO_3-CO_3-CO_2-H_2O system to high ionic strengths at 25°C. Geochimica et Cosmochimica Acta 48(4), 723–751.

Helgeson, H.C., Kirkham, D.H., 1974. Theoretical prediction of the thermodynamic behavior of aqueous electrolytes at high pressures and temperatures. II. Debye–Hückel parameters for activity coefficients and relative partial molal properties. American Journal of Science 274(10), 1199–1261.

Helgeson, H.C., Delany, J.M., Nesbitt, H.W., Bird, D.K., 1978. Summary and critique of the thermodynamic properties of rock-forming minerals. American Journal of Science 278, 1–229.

Königsberger, E., Königsberger, L.C., Gamsjäger, H., 1999. Low-temperature thermodynamic model for the system Na_2CO_3–$MgCO_3$–$CaCO_3$–H_2O. Geochimica et Cosmochimica Acta 63(19-20), 3105–3119.

Krumhansl, J.L., Panenguth, H.W., Zhang, P.-C., Kelly, J.W., Anderson, H.L., Hardesty, J.O., 2000. Behavior of MgO as a CO_2 scavenger at the Waste Isolation Pilot Plant (WIPP), Carlsbad, New Mexico. Materials Research Society Symposium Proceedings 608, 155–160.

Novak, C.F., 1996. Development of the FMT chemical transport simulator: coupling aqueous density and mineral volume fraction to phase compositions. Journal of Contaminant Hydrology 21(1-4), 297–310.

Rai, D., Felmy, A.R. Juracich, S.I., Rao, F.F., 1995. Estimating the hydrogen ion concentration in concentrated NaCl and Na_2SO_4 electrolytes. SAND94-1949. Sandia National Laboratories, Albuquerque, NM.

Rard, J.A., Miller, D.G., 1981. Isopiestic determination of the osmotic and activity coefficients of aqueous $MgCl_2$ solutions at 25°C. Journal of Chemical and Engineering Data 26(1), 38-43.

Robie, R.A., Hemingway, B.S., 1995. Thermodynamic properties of minerals and related substances at 298.15 K and 1 bar (10^5 pascals) pressure and at higher temperatures. United States Geological Survey Bulletin 2131.

Schüssler, W., Metz, V., Kienzler, B., Vejmelka, P., 2002. Geochemically based source term assessment for the Asse salt mine: comparison of modeling and experimental results (Abstract). Programs and Abstracts of Materials Research Society Annual Meeting at Boston, MA, p.713.

Wang, Y., 1998. WIPP PA validation document for FMT, version 2.4. Unpublished report. ERMS# 251587. Sandia National Laboratories, WIPP Records Center, Carlsbad, NM.

Wolery, T.J., 1992. EQ3/6, a software package for geochemical modeling of aqueous systems: package overview and installation guide (version 7.0). UCRL-MA-110662 Pt. I. Lawrence Livermore National Laboratory, Livermore, CA

Wood, S.A., Palmer, D.A., Wesolowski, D.J., Bénézeth, P., 2002. The aqueous geochemistry of the rare earth elements and yttrium. Part XI. The solubility of $Nd(OH)_3$ and hydrolysis of Nd^{3+} from 30 to 290°C at saturated water vapor pressure with in-situ pHm measurement. In: Hellmann, R. and Wood, S.A., (Eds.), Water-Rock Interactions, Ore Deposits, and Environmental Geochemistry: A Tribute to David Crerar, Special Publication 7, The Geochemical Society, pp. 229–256.

Xiong, Y.-L., 2003. Revised thermodynamic properties of brucite determined by solubility studies and its significance to nuclear waste isolation. Abstracts with Programs, Geological Society of America Annual Meeting (Seattle, Washington, November 2–5, 2003) 35(6), 102–103.

Xiong, Y.-L., 2006. Estimation of medium effects on equilibrium constants in moderate and high ionic strength solutions at elevated temperatures by using specific interaction theory (SIT): interaction coefficients involving Cl, OH^- and Ac^- up to 200°C and 400 bars. *Geochemical Transactions* 7(4), doi: 10.118611467-4866-7-4.

Xiong, Y.-L., Snider, A.C., 2003. Experimental investigations of the reaction path in the system MgO–H_2O–CO_2 in concentrated brines at ambient temperature and ambient laboratory atmospheric CO_2: Applications to the Waste Isolation Pilot Plant (Abstract). 2003 Radiochemistry Conference, July 13-16, 2003, Carlsbad, New Mexico, USA. Radiochemistry Society, Richland, WA. Available at http://www.radiochemistry.org/absracts/Experimentalinvestigation.doc, 5/17/05.

Xiong, Y.-L., and Lord, A.S., 2007. Experimental investigations of the reaction path in the MgO–H_2O–CO_2 system in concentrated solutions with ionic strength up to ~7 M at ambient temperature and ambient atmospheric CO_2 and their applications. Submitted to Geochemical Transactions.

Xiong, Y.-L., Wood, S.A., 1999. Experimental determination of the solubility of ReO_2 and the dominant oxidation state of rhenium in hydrothermal solutions. Chemical Geology 158(3-4), 245–256.

Xiong, Y.-L., Wood, S.A., 2001. Hydrothermal transport and deposition of rhenium under subcritical conditions (up to 200°C) in light of experimental studies. Economic Geology 96(6), 1429–1444.

Xiong, Y.-L., Nowak, E.J. and Brush, L.H., 2005. Predicting actinide solubilities in various solutions up to concentrated brines: the Fracture-Matrix Transport (FMT) code. Geochimica et Cosmochimica Acta 69(10), Supp.1, A417.

Table 1. Experimental results from the experiments BRCT-1 starting with deionized (DI) water and BRCT-2 in 0.01M NaCl solution.

Sample number	Run time, hour	$pH_{ob.}$	$m_{Mg^{2+}}$	I_m	$\log \gamma_{Mg^{2+}}$	$\log K^{o\ A}$
BRCT-1-1F	701	10.04	3.31×10^{-3}	9.92×10^{-3}	-1.78×10^{-1}	17.42
BRCT-1-2F	890	10.12	3.34×10^{-3}	1.00×10^{-2}	-1.79×10^{-1}	17.58
BRCT-1-3F	1205	10.06	3.54×10^{-3}	1.06×10^{-2}	-1.84×10^{-1}	17.49
BRCT-1-4F	1633	9.98	2.41×10^{-3}	7.23×10^{-3}	-1.55×10^{-1}	17.19
BRCT-1-5F	1896	10.10	1.88×10^{-3}	5.63×10^{-3}	-1.39×10^{-1}	17.33
BRCT-1-6F	2377	10.15	2.03×10^{-3}	6.09×10^{-3}	-1.44×10^{-1}	17.46
BRCT-1-7F	2879	10.20	1.62×10^{-3}	4.85×10^{-3}	-1.30×10^{-1}	17.48
BRCT-1-8F	3217	10.09	1.67×10^{-3}	5.01×10^{-3}	-1.32×10^{-1}	17.27
BRCT-1-9F	3406	10.05	1.70×10^{-3}	5.10×10^{-3}	-1.33×10^{-1}	17.20
BRCT-1-10F	3550	10.03	1.74×10^{-3}	5.23×10^{-3}	-1.34×10^{-1}	17.17
BRCT-1-11F	3744	10.09	1.22×10^{-3}	3.66×10^{-3}	-1.14×10^{-1}	17.15
BRCT-1-12F	3913	10.01	1.26×10^{-3}	3.79×10^{-3}	-1.16×10^{-1}	17.01
BRCT-1-13F	4222	10.09	1.36×10^{-3}	4.09×10^{-3}	-1.20×10^{-1}	17.20
BRCT-1-14F	4730	10.01	1.49×10^{-3}	4.46×10^{-3}	-1.25×10^{-1}	17.07
BRCT-1-15F	4971	10.07	1.10×10^{-3}	3.29×10^{-3}	-1.09×10^{-1}	17.07
BRCT-1-16F	5475	10.01	1.06×10^{-3}	3.17×10^{-3}	-1.07×10^{-1}	16.94
Average						17.2±0.3 (2σ)
BRCT-2-1F	702	10.05	3.44×10^{-3}	1.69×10^{-2}	-2.67×10^{-1}	17.37
BRCT-2-2F	890	10.13	3.63×10^{-3}	1.73×10^{-2}	-2.70×10^{-1}	17.55
BRCT-2-3F	1205	10.07	3.70×10^{-3}	1.75×10^{-2}	-2.71×10^{-1}	17.44
BRCT-2-4F	1633	10.05	2.41×10^{-3}	1.49×10^{-2}	-2.47×10^{-1}	17.24
BRCT-2-5F	1896	10.03	2.50×10^{-3}	1.51×10^{-2}	-2.49×10^{-1}	17.21
BRCT-2-6F	2377	10.08	2.62×10^{-3}	1.53×10^{-2}	-2.51×10^{-1}	17.33
BRCT-2-7F	2879	10.12	2.03×10^{-3}	1.41×10^{-2}	-2.39×10^{-1}	17.31

BRCT-2-8F	3217	10.05	2.09×10^{-3}	1.42×10^{-2}	-2.40×10^{-1}	17.18
BRCT-2-9F	3406	10.00	2.15×10^{-3}	1.44×10^{-2}	-2.42×10^{-1}	17.09
BRCT-2-10F	3550	10.06	2.23×10^{-3}	1.45×10^{-2}	-2.43×10^{-1}	17.23
BRCT-2-11F	3744	10.08	1.45×10^{-3}	1.30×10^{-2}	-2.27×10^{-1}	17.10
BRCT-2-12F	3913	10.00	1.53×10^{-3}	1.31×10^{-2}	-2.28×10^{-1}	16.96
BRCT-2-13F	4222	10.07	1.66×10^{-3}	1.34×10^{-2}	-2.31×10^{-1}	17.13
BRCT-2-14F	4730	9.98	1.78×10^{-3}	1.36×10^{-2}	-2.34×10^{-1}	16.98
BRCT-2-15F	4791	10.03	1.37×10^{-3}	1.28×10^{-2}	-2.25×10^{-1}	16.97
BRCT-2-16F	5475	10.04	1.51×10^{-3}	1.31×10^{-2}	-2.28×10^{-1}	17.03
Average						17.2±0.3 (2σ)

[A] Equilibrium constants at infinite dilution (log K^{o}) are computed by using measured pH_{ob}, measured $m_{Mg^{2+}}$, and log $\gamma_{Mg^{2+}}$ calculated from the Davies equation, assuming unity for activity of water and brucite. The measured pH_{ob} was not corrected because the ionic strength is so low.

Table 2. Experimental results from the experimental run BRCT-SYN-1 in which brucite was precipitated from 0.1 m $MgCl_2$ solution by dropwise addition of 0.1 m NaOH.

Sample number	Run time, hour	m_{Na^+}	pH_{ob}	m_{H^+}	$m_{Mg^{2+}}$	I_m	log Q	log $K^{o\,A}$
BRCT-SYN-1-1F	24	6.35×10^{-2}	9.34	4.41×10^{-10}	6.27×10^{-2}	2.57×10^{-1}	17.55	17.25
BRCT-SYN-1-2F	214	6.46×10^{-2}	9.32	4.61×10^{-10}	6.40×10^{-2}	2.60×10^{-1}	17.52	17.22
BRCT-SYN-1-3F	333	6.51×10^{-2}	9.27	5.18×10^{-10}	6.20×10^{-2}	2.56×10^{-1}	17.41	17.10
BRCT-SYN-1-4F	480	6.50×10^{-2}	9.37	4.11×10^{-10}	6.20×10^{-2}	2.57×10^{-1}	17.61	17.30
BRCT-SYN-1-5F	695	7.98×10^{-2}	9.37	4.11×10^{-10}	5.37×10^{-2}	2.47×10^{-1}	17.55	17.24
BRCT-SYN-1-6F	864	7.91×10^{-2}	9.24	5.55×10^{-10}	5.23×10^{-2}	2.44×10^{-1}	17.28	16.97
BRCT-SYN-1-7F	1173	7.83×10^{-2}	9.33	4.51×10^{-10}	5.36×10^{-2}	2.46×10^{-1}	17.47	17.16
BRCT-SYN-1-8F	1681	8.42×10^{-2}	9.25	5.42×10^{-10}	5.24×10^{-2}	2.47×10^{-1}	17.30	16.99
BRCT-SYN-1-9F	1922	7.78×10^{-2}	9.30	4.83×10^{-10}	5.16×10^{-2}	2.42×10^{-1}	17.39	17.08
BRCT-SYN-1-10F	2426	7.93×10^{-2}	9.27	5.18×10^{-10}	5.20×10^{-2}	2.44×10^{-1}	17.34	17.03
BRCT-SYN-1-11F	2997	7.82×10^{-2}	9.11	7.48×10^{-10}	5.18×10^{-2}	2.43×10^{-1}	17.02	16.71
BRCT-SYN-1-12F	3433	7.94×10^{-2}	9.14	6.98×10^{-10}	5.31×10^{-2}	2.46×10^{-1}	17.08	16.78
BRCT-SYN-1-13F	3697	8.14×10^{-2}	9.11	7.48×10^{-10}	5.31×10^{-2}	2.47×10^{-1}	17.02	16.72
BRCT-SYN-1-14F	5447	$8.14\times10^{-2\,B}$	9.22	5.81×10^{-10}	6.40×10^{-2}	2.69×10^{-1}	17.32	17.02

BRCT-SYN-1-15F	5856	8.14×10^{-2} [B]	9.51	2.98×10^{-10}	6.04×10^{-2}	2.62×10^{-1}	17.83	17.57
BRCT-SYN-1-16F	8833	8.14×10^{-2} [B]	9.40	3.84×10^{-10}	5.80×10^{-2}	2.57×10^{-1}	17.60	17.34
BRCT-SYN-1-17F	9169	8.14×10^{-2} [B]	9.38	4.02×10^{-10}	5.83×10^{-2}	2.57×10^{-1}	17.56	17.30
BRCT-SYN-1-18F	10776	8.14×10^{-2} [B]	9.48	3.19×10^{-10}	4.27×10^{-2}	2.26×10^{-1}	17.62	17.36
BRCT-SYN-1-19F	11642	8.14×10^{-2} [B]	9.42	3.66×10^{-10}	4.39×10^{-2}	2.29×10^{-1}	17.51	17.25
BRCT-SYN-1-20F	12047	8.14×10^{-2} [B]	9.42	3.66×10^{-10}	4.12×10^{-2}	2.23×10^{-1}	17.49	17.23
BRCT-SYN-1-21F	12284	8.14×10^{-2} [B]	9.42	3.66×10^{-10}	4.33×10^{-2}	2.28×10^{-1}	17.51	17.25
BRCT-SYN-1-22F	13391	8.14×10^{-2} [B]	9.39	3.93×10^{-10}	4.31×10^{-2}	2.27×10^{-1}	17.45	17.19
BRCT-SYN-1-23F	14304	8.14×10^{-2} [B]	9.39	3.93×10^{-10}	4.41×10^{-2}	2.29×10^{-1}	17.46	17.20
BRCT-SYN-1-24F	26692	8.14×10^{-2} [B]	9.29	4.94×10^{-10}	4.52×10^{-2}	2.31×10^{-1}	17.27	17.01
BRCT-SYN-1-25F	35830	8.14×10^{-2} [B]	9.38	4.02×10^{-10}	5.17×10^{-2}	2.44×10^{-1}	17.51	17.25
Average							17.4±0.4(2σ)	17.1±0.4(2σ)

[A] Equilibrium constants at infinite dilution are obtained by using the SIT model for extrapolation based on the interaction coefficients, $\varepsilon(Mg^{2+}, Cl^-)$, and $\varepsilon(H^+, Cl^-)$, recommended by Xiong (2006).

[B] Those values are not measured, and it is assumed that they are similar to that of BRCT-SYN-1-13F.

Table 3. Experimental results from the experimental runs in various NaCl solutions from 0.1 M to 4.0 M.

Sample number	Medium	Run time, h	pH_{ob}	m_{H^+}	$m_{Mg^{2+}}$	m_{OH^-}
BRCT–3–1F	0.1 M NaCl	702	10.08	8.02×10^{-11}	$4.18\pm0.10\times10^{-3}$, A	2.07×10^{-4}
BRCT–3–2F		890	10.22	5.81×10^{-11}	$4.32\pm0.06\times10^{-3}$, A	2.86×10^{-4}
BRCT–3–3F		1205	10.12	7.31×10^{-11}	$4.61\pm0.04\times10^{-3}$, A	2.27×10^{-4}
BRCT–3–4F		1633	10.09	7.84×10^{-11}	$3.04\pm0.10\times10^{-3}$, A	2.12×10^{-4}
BRCT–3–5F		1896	10.04	8.79×10^{-11}	2.96×10^{-3}	1.89×10^{-4}
BRCT–3–6F		2401	10.14	6.98×10^{-11}	3.21×10^{-3}	2.38×10^{-4}
BRCT–3–7F		2879	10.20	6.08×10^{-11}	2.17×10^{-3}	2.73×10^{-4}
BRCT–3–8F		3217	10.09	7.84×10^{-11}	2.28×10^{-3}	2.12×10^{-4}
BRCT–3–9F		3406	10.05	8.59×10^{-11}	2.29×10^{-3}	1.93×10^{-4}
BRCT–3–10F		3550	10.12	7.31×10^{-11}	2.38×10^{-3}	2.27×10^{-4}
BRCT–3–11F		3744	10.14	6.98×10^{-11}	1.66×10^{-3}	2.38×10^{-4}
BRCT–3–12F		3913	10.06	8.39×10^{-11}	1.72×10^{-3}	1.98×10^{-4}
BRCT–3–13F		4222	10.13	7.14×10^{-11}	1.83×10^{-3}	2.32×10^{-4}
BRCT–3–14F		4730	10.04	8.79×10^{-11}	1.88×10^{-3}	1.89×10^{-4}
BRCT–3–15F		4971	10.10	7.66×10^{-11}	1.38×10^{-3}	2.17×10^{-4}
BRCT–3–16F		5476	10.08	8.02×10^{-11}	1.49×10^{-3}	2.07×10^{-4}

BRCT–4–1F	1.0 M NaCl	702	10.00	6.89×10^{-11}	5.48×10^{-3}	2.77×10^{-4}
BRCT–4–2F		890	10.07	5.86×10^{-11}	5.58×10^{-3}	3.26×10^{-4}
BRCT–4–3F		1205	10.03	6.43×10^{-11}	6.01×10^{-3}	2.97×10^{-4}
BRCT–4–4F		1633	9.83	1.02×10^{-10}	4.19×10^{-3}	1.88×10^{-4}
BRCT–4–5F		1896	9.78	1.14×10^{-10}	4.37×10^{-3}	1.67×10^{-4}
BRCT–4–6F		2377	9.84	9.95×10^{-11}	4.38×10^{-3}	1.92×10^{-4}
BRCT–4–7F		2879	9.98	7.21×10^{-11}	3.10×10^{-3}	2.65×10^{-4}
BRCT–4–8F		3216	9.94	7.91×10^{-11}	3.29×10^{-3}	2.42×10^{-4}
BRCT–4–9F		3406	9.84	9.95×10^{-11}	3.32×10^{-3}	1.92×10^{-4}
BRCT–4–10F		3550	9.89	8.87×10^{-11}	3.46×10^{-3}	2.15×10^{-4}
BRCT–4–11F		3744	9.98	7.21×10^{-11}	2.11×10^{-3}	2.65×10^{-4}
BRCT–4–12F		3913	9.90	8.67×10^{-11}	2.26×10^{-3}	2.20×10^{-4}
BRCT–4–13F		4222	9.94	7.91×10^{-11}	$2.44\pm0.00\times10^{-3}$, A	2.42×10^{-4}
BRCT–4–14F		4730	9.86	9.51×10^{-11}	2.71×10^{-3}	2.00×10^{-4}
BRCT–4–15F		4971	9.94	7.91×10^{-11}	2.06×10^{-3}	2.42×10^{-4}
BRCT–4–16F		5476	9.91	8.47×10^{-11}	2.26×10^{-3}	2.25×10^{-4}
BRCT–5–1F	2.0 M NaCl	93	9.78	7.73×10^{-11}	4.70×10^{-3}	1.93×10^{-4}
BRCT–5–2F		309	9.72	8.88×10^{-11}	6.69×10^{-3}	1.68×10^{-4}
BRCT–5–3F		480	9.73	8.67×10^{-11}	4.51×10^{-3}	1.72×10^{-4}

BRCT–5–4F		787	9.71	9.08×10^{-11}	5.21×10^{-3}	1.64×10^{-4}
BRCT–5–5F		1295	9.65	1.04×10^{-10}	5.32×10^{-3}	1.43×10^{-4}
BRCT–5–6F		1536	9.71	9.08×10^{-11}	3.91×10^{-3}	1.64×10^{-4}
BRCT–5–7F		2040	9.67	9.96×10^{-11}	4.14×10^{-3}	1.50×10^{-4}
BRCT–5–8F		2611	9.54	1.34×10^{-10}	4.27×10^{-3}	1.11×10^{-4}
BRCT–5–9F		3047	9.66	1.02×10^{-10}	3.21×10^{-3}	1.46×10^{-4}
BRCT–5–10F		3311	9.56	1.28×10^{-10}	3.48×10^{-3}	1.16×10^{-4}
BRCT–5–11F		5063	9.66	1.02×10^{-10}	3.69×10^{-3}	1.46×10^{-4}
BRCT–5–12F		5470	9.96	5.11×10^{-11}	3.78×10^{-3}	2.92×10^{-4}
BRCT–6–1F	3.0 M NaCl	93	9.71	6.04×10^{-11}	3.64×10^{-3}	1.66×10^{-4}
BRCT–6–2F		309	9.60	7.78×10^{-11}	5.49×10^{-3}	1.29×10^{-4}
BRCT–6–3F		480	9.58	8.15×10^{-11}	4.19×10^{-3}	1.23×10^{-4}
BRCT–6–4F		787	9.59	7.96×10^{-11}	4.67×10^{-3}	1.26×10^{-4}
BRCT–6–5F		1295	9.54	8.93×10^{-11}	5.11×10^{-3}	1.12×10^{-4}
BRCT–6–6F		1536	9.57	8.34×10^{-11}	3.63×10^{-3}	1.20×10^{-4}
BRCT–6–7F		2040	9.53	9.14×10^{-11}	3.92×10^{-3}	1.10×10^{-4}
BRCT–6–8F		2611	9.39	1.26×10^{-10}	3.64×10^{-3}	7.94×10^{-5}
BRCT–6–9F		3047	9.49	1.00×10^{-10}	2.94×10^{-3}	1.00×10^{-4}
BRCT–6–10F		3311	9.44	1.12×10^{-10}	3.13×10^{-3}	8.91×10^{-5}

BRCT–6–11F	5063	9.66	6.78×10^{-11}	3.32×10^{-3}	1.48×10^{-4}
BRCT–6–12F	5470	9.85	4.38×10^{-11}	3.49×10^{-3}	2.29×10^{-4}
BRCT–7–1F	94	9.63	4.70×10^{-11}	3.62×10^{-3}	1.35×10^{-4}
BRCT–7–2F	309	9.52	6.06×10^{-11}	5.28×10^{-3}	1.04×10^{-4}
BRCT–7–3F	480	9.47	6.80×10^{-11}	4.17×10^{-3}	9.32×10^{-5}
BRCT–7–4F	787	9.50	6.35×10^{-11}	4.66×10^{-3}	9.98×10^{-5}
BRCT–7–5F	1295	9.45	7.12×10^{-11}	5.04×10^{-3}	8.90×10^{-5}
BRCT–7–6F	1536	9.47	6.80×10^{-11}	3.21×10^{-3}	9.32×10^{-5}
BRCT–7–7F	2040	9.42	7.63×10^{-11}	3.54×10^{-3}	8.30×10^{-5}
BRCT–7–8F	2611	9.28	1.05×10^{-10}	3.62×10^{-3}	6.02×10^{-5}
BRCT–7–9F	3047	9.38	8.37×10^{-11}	2.81×10^{-3}	7.57×10^{-5}
BRCT–7–10F	3311	9.33	9.39×10^{-11}	2.90×10^{-3}	6.75×10^{-5}
BRCT–7–11F	5063	9.15	1.42×10^{-10}	8.87×10^{-3}	4.46×10^{-5}
BRCT–7–12F	5470	9.53	5.92×10^{-11}	8.74×10^{-3}	1.07×10^{-4}

[A] Replicate analyses.

Table 4. Pitzer interaction parameters and dimensionless standard chemical potentials used in NONLIN modeling

		Binary interaction parameters [A]		
i	j	$\beta^{(0)}$, kg mol^{-1}	$\beta^{(1)}$, kg mol^{-1}	C^{ϕ}, kg^2 mol^{-2}
H^+	Cl^-	0.1775	0.2945	0.0008
Na^+	Cl^-	0.0765	0.2664	0.00127
Na^+	OH^-	0.0864	0.253	0.0044
Mg^{2+}	Cl^-	0.35235	1.6815	0.00519

			Ternary interaction parameters [A]	
i	j	k	θ_{ij}, kg mol^{-1}	Ψ_{ijk}, kg^2 mol^{-2}
Na^+	H^+	Cl^-	0.036	–0.004
Na^+	Mg^{2+}	Cl^-	0.07	–0.012
H^+	Mg^{2+}	Cl^-	0.10	–0.011
OH^-	Cl^-	Na^+	–0.050	–0.006

	Dimensionless standard chemical potentials (μ^o/RT) [A]
H_2O(l)	–95.6635
H^+	0
Na^+	–105.651
Mg^{2+}	–183.468
Cl^-	–52.955
OH^-	–63.435

[A] All binary and ternary interaction coefficients are taken from the compilation of the FMT database (Babb et al., 1996; Babb and Novak, 1997), which is based on Harvie et al. (1984). Dimensionless standard chemical potentials are also from the FMT database (Babb et al., 1996; Babb and Novak, 1997).

Table 5. Dimensionless standard chemical potentials and Gibbs free energies of formation for brucite derived from solubility data of this study in NaCl solutions by using NOLIN

Experimental Data Sets for Modeling	$[\frac{\mu^o}{RT}]_{298.15,\ \text{brucite}}$	$\Delta_f G^o_{298.15,brucite}$ kJ mol^{-1}
BRCT–2–1F, BRCT–3–1F, BRCT–4–1F, BRCT–5–1F, BRCT–6–1F, BRCT–7–1F	–334.883	–830.114
BRCT–2–2F, BRCT–3–2F, BRCT–4–2F, BRCT–5–2F, BRCT–6–2F, BRCT–7–2F	–334.670	–829.586
BRCT–2–3F, BRCT–3–3F, BRCT–4–3F, BRCT–5–3F, BRCT–6–3F, BRCT–7–3F	–334.952	–830.285
BRCT–2–4F, BRCT–3–4F, BRCT–4–4F, BRCT–5–4F, BRCT–6–4F, BRCT–7–4F	–335.295	–831.136
BRCT–2–5F, BRCT–3–5F, BRCT–4–5F, BRCT–5–5F, BRCT–6–5F, BRCT–7–5F	–335.471	–831.572
BRCT–2–6F, BRCT–3–6F, BRCT–4–6F, BRCT–5–6F, BRCT–6–6F, BRCT–7–6F	–335.387	–831.364
BRCT–2–7F, BRCT–3–7F, BRCT–4–7F, BRCT–5–7F, BRCT–6–7F, BRCT–7–7F	–335.421	–831.448
BRCT–2–8F, BRCT–3–8F, BRCT–4–8F, BRCT–5–8F, BRCT–6–8F, BRCT–7–8F	–335.886	–832.601
BRCT–2–9F, BRCT–3–9F, BRCT–4–9F, BRCT–5–9F, BRCT–6–9F, BRCT–7–9F	–335.904	–832.645
BRCT–2–10F, BRCT–3–10F, BRCT–4–10F, BRCT–5–10F, BRCT–6–10F, BRCT–7–10F	–335.776	–832.328
BRCT–2–11F, BRCT–3–11F, BRCT–4–11F, BRCT–5–11F, BRCT–6–11F, BRCT–7–11F	–335.666	–832.055
BRCT–2–12F, BRCT–3–12F, BRCT–4–12F, BRCT–5–12F, BRCT–6–12F, BRCT–7–12F	–335.146	–830.766
Average	–335.36±0.77 (2σ)	–831.3±1.9 (2σ)
$Mg(OH)_2$ (s) + $2H^+ = Mg^{2+} + 2H_2O$	$\log K^o_s$ = 17.2±0.3 (2σ)[A]	

[A] The solubility constant is calculated from the derived average standard Gibbs free energy of formation of brucite in conjunction with the auxiliary data for Mg^{2+}, H_2O(l) and H^+ from Cox et al. (1989).

Table 6. Fugacity of CO_2 gas buffered by the assemblage of brucite and hydromagnesite (5424) at 25 °C by using different Gibbs free energy of formation of brucite.

Buffer Assemblage	Buffer Reaction	$\log f_{CO_2}$ [A]
Brucite–hydromagnesite (5424)	$5Mg(OH)_2(s) + 4CO_2(g) =$ $Mg_5(CO_3)_4(OH)_2 \cdot 4H_2O(s)$	–4.61[B]
	$5Mg(OH)_2(s) + 4CO_2(g) =$ $Mg_5(CO_3)_4(OH)_2 \cdot 4H_2O(s)$	–5.50[C]

[A] In all calculations, thermodynamic data of CO_2(gas) and H_2O(l) are from CODAT (Cox et al., 1989), and the data of hydromagnesite (5424) is from Robie and Hemingway (1995).
[B] The Gibbs free energy of formation of brucite is from Helgeson et al. (1978).
[C] The Gibbs free energy of formation of brucite is from this study.

Table 7. Predicted solubility of Am(III) in a 5 M NaCl solution in equilibrium with brucite-hydromagnesite (5424) at different values of the Gibbs free energy of formation of brucite.

Source of $\Delta_f G^o_{298.15,brucite}$	Solubility-controlling Phase for Am(III)	Predicted Solubility of Am(III)
Helgeson et al. (1978)	$AmOHCO_3$	$Am(CO_3)_3^{3-}$: 1.08×10^{-7} m $Am(CO_3)_2^{-}$: 1.36×10^{-8} m $Am(CO_3)_4^{5-}$: 1.34×10^{-8} m $Am(OH)_2^{+}$: 9.36×10^{-9} m $AmCO_3^{+}$: 1.99×10^{-10} m $Am(OH)_3^{o}$: 1.51×10^{-10} m $AmOH^{2+}$: 2.33×10^{-11} m Am^{3+}: 1.49×10^{-13} m $AmCl^{2+}$: 2.35×10^{-15} m $AmCl_2^{+}$: 9.52×10^{-17} m ΣAm(III): 1.45×10^{-7} m
This Study	$Am(OH)_3$	$Am(CO_3)_3^{3-}$: 1.39×10^{-8} m $Am(CO_3)_2^{-}$: 1.99×10^{-9} m $Am(CO_3)_4^{5-}$: 1.53×10^{-9} m $Am(OH)_2^{+}$: 1.33×10^{-8} m $AmCO_3^{+}$: 3.28×10^{-11} m $Am(OH)_3^{o}$: 5.58×10^{-10} m $AmOH^{2+}$: 1.18×10^{-11} m Am^{3+}: 2.77×10^{-14} m $AmCl^{2+}$: 4.34×10^{-16} m $AmCl_2^{+}$: 1.78×10^{-17} m ΣAm(III): 3.14×10^{-8} m

Figure Captions

Figure 1. A plot showing the attainment of reversal in experiments starting from both undersaturation and supersaturation.

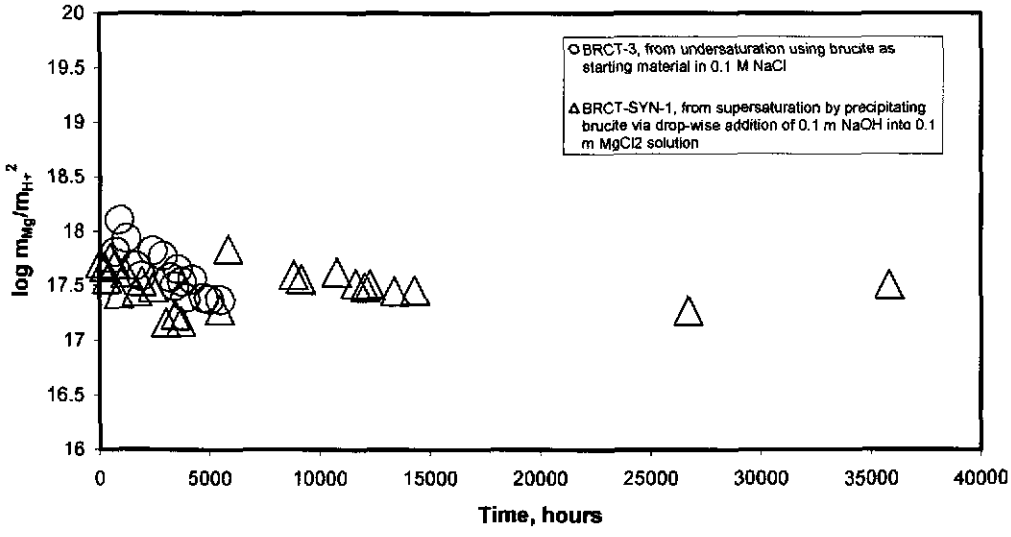

Figure 2. A plot showing all other experimental results starting from undersaturation.